Orientation dependence of temporal and spectral properties of high-order harmonics in solids

Mengxi Wu,[1] Yongsing You,[2] Shambhu Ghimire,[2] David A. Reis,[2] Dana A. Browne,[1]
Kenneth J. Schafer,[1] and Mette B. Gaarde[1,*]

[1]*Department of Physics and Astronomy, Louisiana State University, Baton Rouge, Louisiana 70803-4001, USA*
[2]*Stanford PULSE Institute, SLAC National Accelerator Laboratory, Menlo Park, California 94025, USA*

We investigate the connection between crystal symmetry and temporal and spectral properties of high-order harmonics in solids. We calculate the orientation-dependent harmonic spectrum driven by an intense, linearly polarized infrared laser field, using a momentum-space description of the generation process in terms of strong-field-driven electron dynamics on the band structure. We show that the orientation dependence of both the spectral yield and the subcycle time profile of the harmonic radiation can be understood in terms of the coupling strengths and relative curvatures of the valence band and the low-lying conduction bands. In particular, we show that in some systems this gives rise to a rapid shift of a quarter optical cycle in the timing of harmonics in the secondary plateau as the crystal is rotated relative to the laser polarization. We address recent experimental results in MgO [Y. S. You *et al.*, Nat. Phys. **13**, 345 (2017).] and show that the observed change in orientation dependence for the highest harmonics can be interpreted in the momentum space picture in terms of the contributions of several different conduction bands.

I. INTRODUCTION

High-order-harmonic generation (HHG) in transparent crystals has attracted much attention recently given its potential as a bright, compact, and easily controllable source of extreme utraviolet (XUV) radiation [1–8]. The dominant generation mechanism has been shown to be substantially different from that of HHG in gases [1,2,6,9]. Given the spatial periodicity of crystals, the process is well suited to a momentum (k) space picture, by considering the electron dynamics on the band structure that takes place each half-cycle of the driving field: (i) tunneling from the valence band (VB) to the conduction band (CB); (ii) acceleration on the CB, which will give rise to an intraband current; and (iii) a time-dependent coherence between the VB and the CB at the momentum of the electron gives rise to an interband polarization with a time-varying frequency [2,9–12]. In Ref. [11] we showed that this picture can be reproduced for a one-dimensional system by considering the electron dynamics in terms of a driven multilevel system that originates at the high-symmetry Γ point of the band structure. This is because the field-dressed states of such a system exactly reproduce the full band structure they originate from, and the acceleration to a certain k on the lowest CB is therefore equivalent to the evolution of the energy of the first-excited field-dressed state in the time-dependent field.

The momentum-space description of crystal HHG suggests a close connection between the band structure and the harmonic spectrum: (i) since both the interband and the intraband contribution to the signal rely on moving population to the conduction band via tunneling, the size of the minimum band gap will strongly influence the harmonic yield [9,11,13]; (ii) the cutoff energy of the primary (or secondary) plateau from the interband contribution will be determined by the maximum band gap between the VB and the first (second) CB [6,9,11]; and (iii) the curvature of the conduction band will control both the cutoff energy of the intraband emission [1,7] and the attochirp of the interband emission [5,8,11].

In this paper we show that the spectral and temporal properties of crystal harmonics can be controlled via the band structure, specifically as the crystal is rotated with respect to the laser polarization. We also show that the equivalence between the band structure and the field-dressed states of a multilevel system that originates from its Γ point can be extended to two dimensions and three dimensions by using coupling matrix elements of the momentum operator projected onto the polarization direction. This allows us to very simply interpret the orientation dependence and the intensity dependence of the HHG in terms of the properties of the band structure. We discuss how this connects with other recent real- and momentum-space interpretations of crystal HHG orientation dependence as observed in experiments [1,2,6,14–16] and calculations [16–19].

We begin by considering the simplest possible periodic structure that has an orientation dependence, namely a two-dimensional (2D) square lattice, interacting with a linearly polarized midinfrared (MIR) laser field. The lattice spacing is chosen such that the band gap is 6.6 eV and the system has a second low-lying conduction band [see Fig. 1(a)] and thus exhibits both a primary and a secondary plateau even at moderate intensities. The curvature of the second CB has opposite signs along the Γ-X and the Γ-M directions and we show that this gives rise to a rapid shift of a quarter optical cycle in the timing of harmonics in the secondary plateau as the crystal is rotated relative to the laser polarization. Next, we consider recent experimental results on the orientation dependence of harmonics in single-crystal MgO [14]. We show that the observed change in the orientation dependence starting at harmonic 19 (H19) can be attributed to the contribution from a higher-lying CB which in this case is primarily reached in the Γ-X direction, as opposed to the lowest-lying CB which is more strongly coupled in the Γ-K direction.

II. RESULTS FOR 2D SQUARE LATTICE

Our theoretical approach is described in detail in Refs. [11,20]. Briefly, we solve the time-dependent
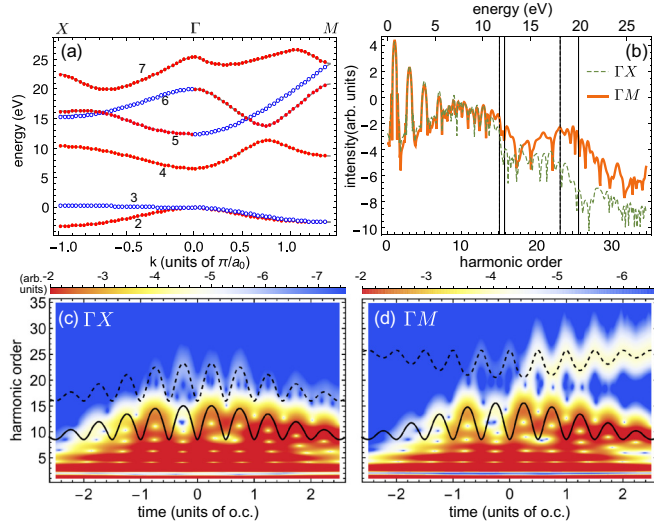
_____
*gaarde@phys.lsu.edu

FIG. 1. (a) Dotted lines show the band structure for the 2D square crystal. Only bands with the same color have dipole-allowed couplings. (b) Harmonic spectra along Γ-X (thin dashed line) and Γ-M (thick solid line), generated by a 1600-nm, 3.0 TW/cm^2 laser pulse (shown in log scale). Vertical solid (dashed) lines indicate the maximum VB-CB separations that can be reached in the two lowest red CBs in the Γ-X (Γ-M) direction. (c), (d) Time-frequency plots of the harmonic emission polarized along (c) Γ-X and (d) Γ-M. Time is in units of optical cycles (o.c.). Solid (dashed) lines in panels (c) and (d) indicate the instantaneous band gap between the VB and the lowest (next-lowest, dipole-coupled) CB.

Schrödinger equation for an electron in a periodic potential in the velocity gauge, by expanding the time-dependent wave function in a basis of Bloch states, $|\psi_{\mathbf{k}}(t)\rangle = \sum_n C_{n\mathbf{k}}(t)|\phi_{n\mathbf{k}}\rangle$. The Bloch states $|\phi_{n\mathbf{k}}\rangle$ are the eigenstates of the field-free Hamiltonian and form the band structure, with n representing the band and $\mathbf{k}$ representing a particular crystal momentum in the first Brillouin zone. In the velocity gauge the different $\mathbf{k}$ channels remain uncoupled even in the presence of the laser field, and the harmonic spectrum from each $\mathbf{k}$ is calculated independently as the Fourier transform of the time-dependent current $j_{\mathbf{k}}(t) = -[\langle\psi_{\mathbf{k}}(t)|\hat{\mathbf{p}}\cdot\hat{\mathbf{e}}|\psi_{\mathbf{k}}(t)\rangle] + A(t)$ (in atomic units). Here, $A(t)$ is the vector potential of the laser field which is linearly polarized along unit vector $\hat{\mathbf{e}}$, and the matrix elements of the momentum operator $\hat{\mathbf{p}}$ (projected onto $\hat{\mathbf{e}}$) are calculated from the Bloch states. Contributions from multiple $\mathbf{k}$ channels are added coherently. Although we discuss results that include multiple k-points, in the figures below we show only the contribution from the high symmetry Γ point such that $\mathbf{k}_0 = 0$, where the tunneling probability is maximized, corresponding to an initial wave function which is spatially delocalized. In all calculations below, the laser pulse is described by a vector potential of the form $A_0 f(t) \sin(\omega t)$, where A_0 is the peak vector potential, ω is the laser frequency, and the envelope $f(t) = \cos^4(\frac{\omega t}{22})$ corresponds to a full-width-at-half-maximum pulse duration of approximately three optical cycles.

We start by exploring HHG from a 2D square lattice described by the potential $V(x,y) = -0.5(1 - \cos 2\pi x/a_x)(1 - \cos 2\pi y/a_y)$, with lattice constant $a_x = a_y = a_0 = 6$ a.u. The Bloch states and dipole couplings for this

Mathieu-type potential can be calculated exactly. Figure 1(a) shows the band structure along the two different symmetry directions for this potential: Γ-X (parallel to the edges) and Γ-M (along the diagonal). We note that, as explained in more detail in the next paragraph, along these two symmetry directions the bands can be divided into two groups, colored red (closed) and blue (open), where the bands in each group have nonzero coupling matrix elements only to other bands in that group—i.e., so that the red (blue) bands only couple to other red (blue) bands. We treat the lowest band from each group (bands 2 and 3) as valence bands with initial population. However, since the lowest red CB 4 is much lower than the lowest blue CB (6 along Γ-X, 5 along Γ-M) we expect the harmonic generation dynamics will be dominated by the red group. Band 1 is much lower than bands 2 and 3 and plays no role in the HHG dynamics.

This grouping of the bands arises because of the symmetry of the Hamiltonian with respect to a reflection in the plane that contains $\mathbf{k}$. In particular, the component of the momentum operator along each of these directions, $\mathbf{k} \cdot \mathbf{p}$, is the term in the Hamiltonian that causes the transitions between bands, and it is invariant under this reflection [which has the form $(x \to x, y \to -y)$ along Γ-X and $(x \leftrightarrow y)$ along Γ-M]. The wave functions along $\mathbf{k}$ can therefore be classified as even or odd under this symmetry operation, so that only states of the same symmetry will be coupled. Along any direction other than Γ-X and Γ-M, the wave functions will be superpositions of states from each symmetry group and cannot as such be characterized as red or blue.

We also calculate the adiabatic (field-dressed) states of a multilevel system that consists of only the $k = 0$ elements on the band structure; i.e., we calculate the eigenstates of the field-dependent Hamiltonian [11]:

$$H(A\hat{\mathbf{e}}) = H_0 + A\hat{\mathbf{e}} \cdot \hat{\mathbf{p}} + A^2/2. \quad (1)$$

To compare the energies of these states to the band structure we let the vector potential play the role of $\mathbf{k}$ so that $\mathbf{k} = \mathbf{k_0} + A\hat{\mathbf{e}}$, reflecting that the component of the vector potential in a given direction is the momentum that would be imparted to an electron starting from $\mathbf{k_0}$. The agreement between the band structure and the adiabatic state energies (shown with thin solid lines) is so good throughout the 2D Brillouin zone that they cannot be distinguished from each other in Fig. 1(a). An important conclusion from this agreement is that we can interpret the orientation-dependent dynamics of the electron on the 2D band structure in terms of the field-dressed states for a multilevel system representing the Γ point, as long as we take into account the polarization direction relative to the crystal orientation.

Next we calculate the harmonic spectra generated by a 1600-nm, 3.0 TW/cm^2 laser pulse, linearly polarized along the Γ-X or the Γ-M direction, as shown in Fig. 1(b). Both spectra exhibit a two-plateau structure with a primary plateau that extends to approximately H15 ($\approx$ 12 eV) and a weaker, secondary plateau. The primary plateau is due to the coupling between bands 2 and 4. Its strength is determined by the separation and the curvature of bands 2 and 4 at the minimum band gap (via the tunneling probability, see Ref. [11]), and its cutoff energy is determined by the maximum separation between the bands that can be reached by vector-potential

driven acceleration on band 4, which in this case is equal to the maximum band gap. This is illustrated by the excellent agreement between the cutoff energies and the vertical lines. Both of these energies are similar along Γ-X and Γ-M, which leads to primary plateaus of similar strength and cutoff energy. However, the secondary plateau is both more intense and extends further in the Γ-M spectrum. This is because the secondary plateau is due to the coupling between the VB and the second CB (CB2) which is reached in a stepwise process from CB1. The minimum 4–6 band gap is much smaller along Γ-M than the 4–5 gap along Γ-X, thus giving the higher yield in this direction. Furthermore, the maximum 4–6 separation along Γ-M is larger than the 4–5 separation along Γ-X, leading to the higher cutoff energy.

We note that the orientation dependence in the strength of the secondary plateau is preserved in calculations using an initially "filled" valence band (including contributions from all **k**, not shown). For both orientations, the full valence band results in a suppression of the primary plateau relative to the secondary plateau (and a strong suppression of the intraband harmonics 5–9). For the Γ-M direction this results in primary and secondary plateaus of similar strength. In the Γ-X direction, the secondary plateau is weaker by about an order of magnitude. Thus, for this system, meaningful information about the orientation dependence can indeed be extracted from the calculations originating at the Γ point.

We can get additional insight into the dynamics on the band structure by considering the time-frequency profile of the harmonic radiation in the two directions as shown in Figs. 1(c) and 1(d), calculated using a wavelet transform [21]. We note that in the Γ-M direction, the secondary plateau emission is shifted by a quarter cycle relative to the primary plateau; this is not the case in the Γ-X direction. These emission times are very well reproduced by the instantaneous 2–4 and 2–5 (or 2–6 along Γ-M) band gaps shown in Figs. 1(c) and 1(d). We can understand this behavior in terms of the dynamics of the electron on the band structure: (i) the 2–4 tunneling in both polarization directions happens at the minimum band gap at $k = 0$, i.e., at the zero of the vector potential, and each harmonic in the primary plateau is emitted twice during each half-cycle as the vector potential accelerates the electron up the CB and then back down. (ii) in the Γ-X direction, the minimum 4–5 band gap is at $k = 0$ and leads to the same dynamics in the secondary plateau as in the primary plateau. However, in the Γ-M direction the minimum 4–6 band gap occurs away from $k = 0$, at $k = 0.8\pi/a_0$. This means that the 4–6 tunneling will happen near the maximum of the vector potential (which at this intensity corresponds to $k = 0.6\pi/a_0$), and each harmonic is emitted twice during the half-cycle as the vector potential decelerates the electron to $k = 0$ and back up.

The difference between the results in Figs. 1(c) and 1(d) suggests that the subcycle time structure of the EUV light from this system can be controlled by rotating it relative to the polarization direction. We return to this point in more detail below.

We next explore the orientation dependence of the harmonic yield in more detail. Figure 2(a) shows the orientation dependence of the entire spectrum, on a log scale, at a peak intensity of 3.0 TW/cm^2. As discussed above, the harmonics in the primary plateau do not exhibit a strong orientation dependence: the radiation around 0° and 90° (the Γ-X direction) is emitted

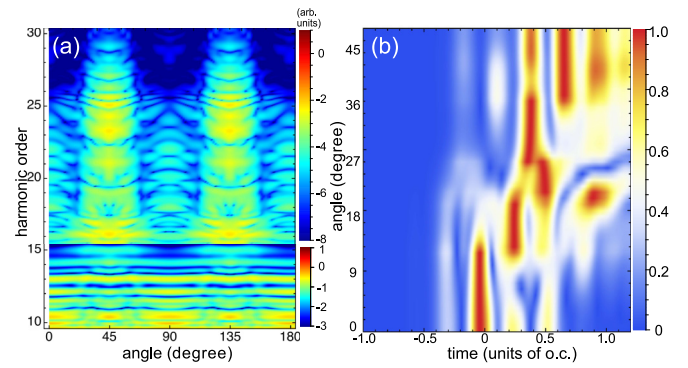
FIG. 2. (a) Orientation dependence of the harmonic spectrum for peak intensity 3.0 TW/cm^2 (shown in log scale). Note that the color scale is different for the harmonics below and above H15. (b) Time profile of emission near H25, as a function of angle (linear scale, and normalized at each angle for clarity).

in broad structures and is generally stronger than that at 45° (the Γ-M direction). In contrast, the harmonics in the secondary plateau are strongly peaked around 45° (the Γ-M direction). For almost all the harmonics in the spectrum, in both the primary and secondary plateau, the yield is minimized at angles far from the high-symmetry directions Γ-X and Γ-M. This can be understood by considering the (lack of) symmetry properties of the wave functions at these angles—these wave functions will have both red state character and blue state character, and the contribution to the harmonic yield is much lower from the blue states because the lowest blue conduction band is so much higher than the lowest red conduction band.

Figure 2(b) shows how the orientation dependence of the second plateau is reflected in the subcycle time profile of radiation centered on H25, which is near the cutoff of the secondary plateau. Similar to the result in Figs. 1(c) and 1(d), we see that the timing of this EUV radiation depends strongly on orientation, with a rapid time shift between 20° and 25° from emission near the quarter-cycle to emission near the half-cycle. This shift originates in the fact that the tunneling time between the lowest and the next-lowest conduction bands happens at two different times in the Γ-X and Γ-M directions, specifically that the tunneling in the Γ-X direction happens near the peak (rather than the zero) of the vector potential, when the electron on CB4 sees the lowest band gap to CB6. In an experiment, such a shift would correspond to being able to control the subcycle timing of the EUV with attosecond precision by rotating the crystal relative to the laser polarization. We note that, although in our system H25 is much weaker along the Γ-X direction than along the Γ-M direction, this would not in general be true, since the relative timing is controlled by *where* in the Brillouin zone the band gap is minimized, and the relative strength is controlled by the *size* of the minimum band gap.

We next consider how the orientation dependence of the harmonic spectrum depends on the laser intensity. Figures 3(a) and 3(b) show the harmonic spectrum (in log scale) as a function of laser intensity, and Fig. 3(c) shows the orientation-dependent yield of H21 on a linear scale, calculated for three different intensities. Figures 3(a) and 3(b) show that at the lowest intensities where the second plateau is visible,
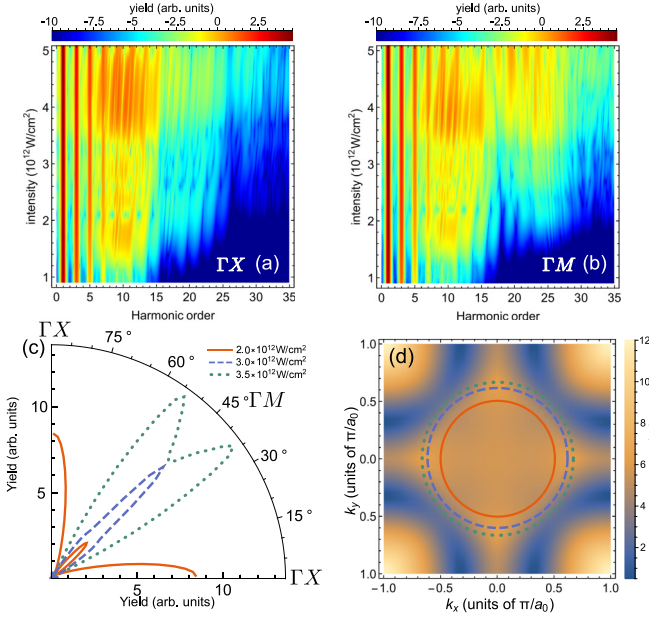
FIG. 4. (a) Band structure for the rectangular crystal (see text), along the Γ-X and Γ-Y symmetry directions. Only bands with the same color have dipole-allowed couplings. (b) Harmonic spectra along Γ-X (thick solid line) and Γ-Y (thin dashed line), generated by a 6 TW/cm^2 laser pulse.

FIG. 3. Intensity dependent harmonic spectra along Γ-X (a) and Γ-M (b), shown in log scale. Panel (c) shows the orientation dependence of H21 for peak intensities of 2.0 TW/cm^2 (red solid line, ×1000), 3.0 TW/cm^2 (blue dashed line, ×10), and 3.5 TW/cm^2 (green dotted). (d) CB1-CB2 energy separation throughout the first Brillouin zone. Circles indicate the maximum k-values that can be reached at the intensities in panel (b).

it is actually stronger in the Γ-X direction than in the Γ-M direction. This is because for low field strengths, the electron does not reach large k-values in band 4 and the tunneling to the next CB therefore happens close to $k = 0$, at which the 4–5 band gap is much smaller in the Γ-X direction than the 4–6 gap in the Γ-M direction. Only when the field is strong enough to accelerate the electron close to the minimum band gap along Γ-M does the second-plateau yield become stronger in this direction [22]. This is reflected in the orientation dependence of H21, in the middle of the secondary plateau [Fig. 3(c)], which changes rapidly with intensity: At intensities below about 2.5 TW/cm^2, H21 is peaked along 0° and 90°, whereas it is sharply peaked around 45° at 3.0 TW/cm^2. At even higher intensity, the yield has a double-peak structure centered on 45° which cannot be explained just by looking at the behavior in Figs. 3(a) and 3(b). Instead we show in Fig. 3(d) the orientation-dependent band gap between CB4 and the next-lowest conduction band [23]. Here, the circles mark the maximum k-values that can be reached at the different intensities, starting from $k = 0$ at the zero of the vector potential. At moderate intensities (between 2.5 and 3.0 TW/cm^2), the minimum band gap is reached at 45°, giving rise to the sharp peaks at this angle in Fig. 2(c), whereas at higher intensities it is reached at two angles below and above 45°, giving rise to the double-peak structure in Fig. 2(d).

Up to now, we have seen that the square crystal considered above has such a high degree of symmetry that the primary plateau is relatively independent of orientation. This is different from many of the systems that have been studied experimentally [1,14–16]. For a 2D system we can break this symmetry by considering a rectangular crystal so that
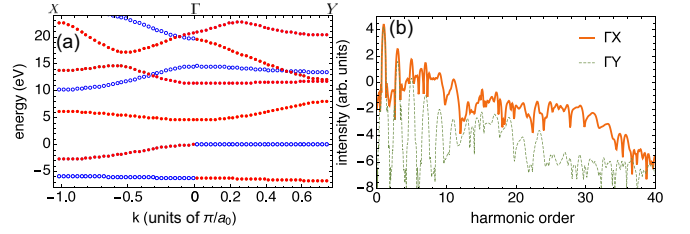
$a_x = 6 \neq a_y = 8$ a.u. in the Mathieu potential used above. The band structure for this system is shown in Fig. 4(a), and Fig. 4(b) shows harmonic spectra generated by a 1600-nm, 6.0 TW/cm^2 laser pulse. We see that, in general, the shallower potential in the y direction leads to a much larger spacing between the VB and the lowest dipole-coupled CB, and this in turns causes the harmonic spectrum in the Γ-X direction to both be much stronger and have a higher cutoff energy than that in the Γ-Y direction.

III. RESULTS IN MgO

Finally, we consider the orientation dependence of a more realistic system, namely single-crystal MgO as was recently characterized experimentally in Ref. [14]. We start by calculating the band structure and coupling matrix elements, using density functional theory via the WIEN2K sofware package [24] as described in Ref. [8]. Figure 5(a) shows the band structure along Γ-X and Γ-K, corresponding to the Mg-O and Mg-Mg nearest-neighbor directions. The bands are color-coded so that only bands of the same color couple to each other along the directions shown. We include the 13 bands shown in Fig. 5(a) in the calculation and treat bands 6, 7, and 8 as valence bands that have initial population. We include a rapid dephasing of the conduction band population by adding the energy-dependent decay rate $\gamma_n = 0.05 E_n$ to the calculation, where E_n is the energy of band n at the Γ point [9], in atomic units. We rotate the laser polarization in the plane containing Γ-X and Γ-K and show the $\mathbf{k_0} = 0$ contribution to the orientation-dependent spectrum in Fig. 5(b), calculated using a 1300-nm, 20 TW/cm^2 laser pulse. Figure 5(c) shows lineouts from Fig. 5(b) for a few select harmonics, on a linear scale. Figure 5(d) shows experimental results measured under similar conditions, although with a longer pulse duration (reprinted from Ref. [14]). It is clear from both the theory and the experiment that the orientation dependence, which has fourfold symmetry, changes dramatically with increasing harmonic order. In both theory and experiment the harmonics from H19 and above are sharply peaked primarily along 0° (Γ-X), with the experiment exhibiting additional smaller and rapidly decreasing peaks along 45° (Γ-K). In the experiment, harmonics from H17 and below exhibit distinct peaks at both 0° and 45°. These peaks have comparable intensity and remain sharp along 0° but with broader features in the 45° direction. In the calculation shown in Figs. 5(b) and 5(c), harmonics
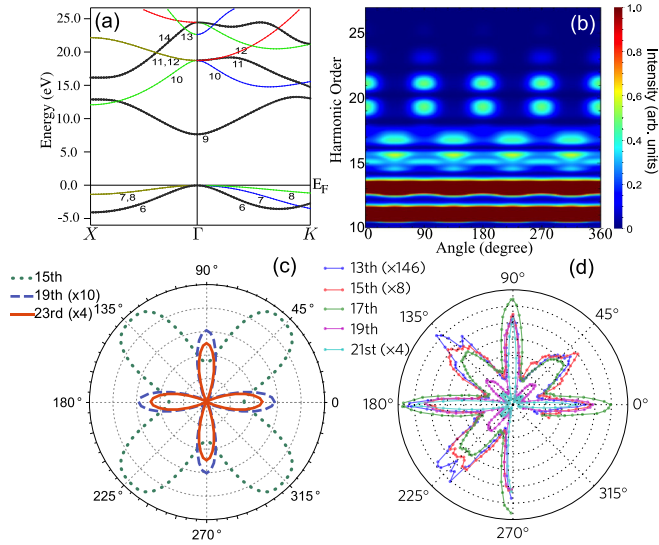
FIG. 5. (a) Band structure of MgO, calculating using DFT. (b), (c) Calculated orientation-dependent spectra (b) and lineout of individual harmonics (c) for rotation in the Γ-X and Γ-K plane, for a 1300-nm, 20 TW/cm^2 pulse. (d) Experimentally measured yields for a range of harmonics, reprinted from Ref. [14].

below H17 are predominantly in the 45° direction, with broad (nonzero) minima at 0°.

The calculated results in Figs. 5(b) and 5(c) can be interpreted in terms of the orientation-dependent band structure, in particular considering the contribution from the group of bands colored black (thick), which have the lowest-lying conduction band 9. The primary plateau extends to H17 and is produced by the coupling between bands 6 and 9, which are similar in the Γ-X and Γ-K directions. In the calculation, the slightly steeper curvature of band 6 in the Γ-K direction gives rise to a larger coupling matrix element and thereby a higher tunneling probability for this orientation than along Γ-X [11,20]. Energies from 20–25 eV (H21 and above) are most easily accessed in the Γ-X direction from band 14, which gives rise to the sharp peaks around 0° and 90°. The fact that in the experiment, H19 and H21 are also primarily reached in a small cone of angles around 0° and 90° suggests that the experiment is indeed probing the orientation-dependent band structure and, in particular, that the second conduction band is reached more easily in the Γ-X direction than in the Γ-K direction. We also note that the general observation of minimal harmonic yield away from the high-symmetry directions in both experiment and theory is consistent with the symmetry properties of the bands, as also discussed in the context of Fig. 2(a): away from the Γ-X and Γ-K directions the character of the bands is mixed and the transition probability to the lowest-lying conduction band 9 will decrease.

The calculated orientation dependence in Fig. 5(c) shows less structure than in the experiment, exhibiting broad nonzero minima at 0° and 90° rather than individual peaks. We believe this is due to including only the contribution from the Γ point in the harmonic yield, which means that the orientation dependence tends to follow the smoothly varying 3D band structure. If we include a small range of **k** values near the Γ point (20% in each direction), we observe sharper

features in the orientation dependence of the lower harmonics (not shown), although still not in exact agreement with the experimental peaks. This suggests that the sharp features arise from interference between contributions from slightly different k-values in the Brillouin zone.

IV. SUMMARY AND PERSPECTIVE

Our results in general, and the previous two paragraphs in particular, stress that quantitative comparisons between experiment and theory require accurate calculations that include a number of valence and conduction bands. In principle, a full solution of the crystal structure should yield eigenvalues $\epsilon_n(\mathbf{k})$ and Bloch states $|\phi_{n\mathbf{k}}\rangle$ at a level of convergence such that the band structure derived from the adiabatic states [Eq. (1)] would be fully consistent with the "normal" band structure derived from the eigenvalues. In practice, the energies and momentum matrix elements from sophisticated structure codes such as WIEN2K are calculated with separate levels of accuracy for each k-value. It is not surprising therefore, that in MgO the adiabatic states we generate from the Γ-point band-structure elements do not exactly reproduce the full band structure, in particular for k-values larger than $\approx 0.5\pi/a_0$.

Our 2D calculations using the Mathieu potential, for which we can generate fully consistent solutions for any k, have shown us that the band structure can indeed be used to infer many properties of the harmonic emission, such as the orientation-dependent yield, cutoff energies, and time profiles. If we apply this knowledge directly to the case of MgO, then the band structure in Fig. 5(a) suggests that the timing of the XUV emission is similar to that observed in Fig. 1(d), in which harmonics in the second plateau are shifted by a quarter-cycle relative to those in the first plateau. Likewise, we predict that any system in which the shapes of similar-energy conduction bands are concave along one crystal direction and convex along another will allow for subcycle control of the XUV emission time by rotating the crystal relative to the laser polarization. In MgO, our calculations are ambiguous on this point due to the abovementioned problem reconstructing the outer edges of the Brillouin zone. Our results indicate that additional information about the band structure beyond the lowest conduction band may be gained from accurate measurements of the spectral and temporal properties of the high harmonics.

In summary, we have discussed how the orientation-dependent yield and cutoff energies can be understood in a momentum-space picture in terms of interband and intraband dynamics on the band structure. Our momentum space picture, similarly to that of Refs. [18,19], provides a useful complement to the picture of strong-field-driven electron trajectories discussed in real space in Refs. [14,17] and in momentum space in Ref. [15]. In particular, the real-space picture in Ref. [14] provided an intuitive sense of which crystallographic directions are more favorable for HHG in terms of coherent collision of driven electrons to first and second nearest-neighbor sites. Similarly, in Ref. [16] the experimental results are discussed in terms of directions in real space whereas the accompanying calculations are based in momentum space. Since the band structure corresponds to the momentum-space representation of the real-space crystal structure one should of course be able to describe the same

physics in both spaces. A fruitful area of exploration might thus be toward a picture of HHG in crystals that can be interpreted in both real space and momentum space.

[1] S. Ghimire, A. D. DiChiara, E. Sistrunk, P. Agostini, L. F. DiMauro, and D. A. Reis, Nat. Phys. **7**, 138 (2011).

[2] O. Schubert, M. Hohenleutner, F. Langer, B. Urbanek, C. Lange, U. Huttner, D. Golde, T. Meier, M. Kira, S. W. Koch, and R. Huber, Nat. Photonics **8**, 119 (2014).

[3] T. T. Luu, M. Garg, S. Y. Kruchinin, A. Moulet, M. T. Hassan, and E. Goulielmakis, Nature (London) **521**, 498 (2015).

[4] M. Hohenleutner, F. Langer, O. Schubert, M. Knorr, U. Huttner, S. W. Koch, M. Kira, and R. Huber, Nature (London) **523**, 572 (2015).

[5] G. Vampa, T. J. Hammond, N. Thiré, B. E. Schmidt, F. Légaré, C. R. McDonald, T. Brabec, and P. B. Corkum, Nature (London) **522**, 462 (2015).

[6] G. Ndabashimiye, S. Ghimire, M. Wu, D. A. Browne, K. J. Schafer, M. B. Gaarde, and D. A. Reis, Nature (London) **534**, 520 (2016).

[7] M. Garg, M. Zhan, T. T. Luu, H. Lakhotia, T. Klostermann, and A. G. E. J. Goulielmakis, Nature (London) **538**, 359 (2016).

[8] Y. S. You, M. Wu, Y. Yin, A. Chew, X. Ren, S. Gholam-Mirzaei, D. A. Browne, M. Chini, Z. Chang, K. J. Schafer, M. B. Gaarde, and S. Ghimire, Opt. Lett. **42**, 1816 (2017).

[9] G. Vampa, C. R. McDonald, G. Orlando, D. D. Klug, P. B. Corkum, and T. Brabec, Phys. Rev. Lett. **113**, 073901 (2014).

[10] T. Higuchi, M. I. Stockman, and P. Hommelhoff, Phys. Rev. Lett. **113**, 213901 (2014).

[11] M. Wu, D. A. Browne, K. J. Schafer, and M. B. Gaarde, Phys. Rev. A **94**, 063403 (2016).

[12] T. Otobe, Phys. Rev. B **94**, 235152 (2016).

[13] P. G. Hawkins and M. Y. Ivanov, Phys. Rev. A **87**, 063842 (2013).

[14] Y. S. You, D. A. Reis, and S. Ghimire, Nat. Phys. **13**, 345 (2017).

[15] H. Liu, Y. Li, Y. S. You, S. Ghimire, T. F. Heinz, and D. A. Reis, Nat. Phys. **13**, 262 (2017).

[16] F. Langer, M. Hohenleutner, U. Huttner, S. W. Koch, M. Kira, and R. Huber, Nat. Photonics **11**, 227 (2017).

[17] S. A. Sörngård, S. I. Simonsen, and J. P. Hansen, Phys. Rev. A **87**, 053803 (2013).

[18] N. Tancogne-Dejean, O. D. Mücke, F. X. Kärtner, and A. Rubio, Phys. Rev. Lett. **118**, 087403 (2017).

[19] N. Tancogne-Dejean, O. D. Mücke, F. X. Kärtner, and A. Rubio, Nat. Commun. **8**, 745 (2017).

[20] M. Wu, S. Ghimire, D. A. Reis, K. J. Schafer, and M. B. Gaarde, Phys. Rev. A **91**, 043839 (2015).

[21] Wolfram Research Inc., MATHEMATICA 11.0 (2016), see ContinuousWaveletTransform.

[22] At the highest intensities, a third plateau is visible in both harmonic spectra at energies exceeding the maximum separation between the VB and the second CB. This plateau originates in coherences between the VB and the third CB and requires an additional tunneling from the second to the third CB.

[23] Note that for low intensity in the Γ-M direction this is the blue band in Fig. 1(a) which does not couple to band 4.

[24] P. Blaha, K. Schwarz, G. Madsen, D. Kvasnicka, and J. Luitz, WIEN2K: *An Augmented Plane Wave + Local Orbitals Program for Calculating Crystal Properties* (Karlheinz Schwarz, Technische Universität Wien, Austria, 2001).